HELIOTOMOGRAPHY OF THE OUTER LAYERS OF THE SUN

A. G. Kosovichev[1], T. L. Duvall, Jr.[2], A. C. Birch[1], L. Gizon[1], P. H. Scherrer[1], and Junwei Zhao[1]

[1]W.W. Hansen Experimental Physics Laboratory, Stanford University, Stanford, CA, USA
[2]Laboratory for Astronomy and Solar Physics, NASA/GSFC, Greenbelt, MD, USA

ABSTRACT

Heliotomography offers important diagnostics of the solar interior by providing three-dimensional maps of the sound speed and flows in the upper convection zone. These diagnostics are based on inversion of travel times of acoustic waves which propagate between different points on the solar surface through the interior. The most significant variations in the thermodynamic structure found by this method are associated with sunspots and complexes of solar activity. The inversion results provide evidence for areas of higher sound speed beneath sunspot regions located at depths of 4-20 Mm, which may be due to accumulated heat or magnetic field concentrations. The results reveal structures and flows associated with active regions and sunspots at various stages of their evolution, and provide important constraints for theories of solar dynamics and activity.

Key words: heliotomography, time-distance helioseismology, solar interior, active regions, sunspots.

1. INTRODUCTION

In this paper we present a brief review of recent developments in heliotomography. Most efforts in heliotomography have been focused on developing a rigorous methodology based on a wave theory which provides an accurate procedure for data interpretation and inversion, and on investigating potentials of heliotomography for diagnostics of solar variability. Most of these diagnostics which employed a traditional time-distance technique based on a theoretical-ray approximation are more qualitative than quantitative. Nevertheless, they have provided important new insights into the internal mechanisms of solar variability (Kosovichev, Duvall and Scherrer, 1999). Of course, the ultimate goal of these investigations is to merge these directions and provide a robust diagnostic tool for both understanding the physics of solar variability and space weather forecasts.

We review the principles and new approaches in the method of heliotomography, among which are "deep focusing" schemes for diagnostics of the deep interior and even the far-side of the Sun, and a method for calculating sensitivity kernels, based on the Born approximation to the wave equation. This method essentially represents a 3-D generalization of the "global" 2-D helioseismology based on normal mode frequencies. We also discuss the recent result for diagnostics of emerging active regions, large-scale complexes of activity and associated mass flows, structure and dynamics of a large sunspot, and relations of these diagnostics to irradiance variations.

2. METHODS OF HELIOTOMOGRAPHY

Solar acoustic waves are excited by turbulent convection near the solar surface and propagate through the interior with the speed of sound. Because the sound speed increases with depth the waves are refracted and reappear on the surface at some distance from the source. The wave propagation is illustrated in Figure 1a. Waves excited at point A will reappear at the surface points B, C, D, E, F, and others after propagating along the ray paths indicated by curves.

The basic idea of solar tomography is to measure the acoustic travel time between different points on the solar surface, and then to use these measurements to infer variations of the structure and flow velocities in the interior along the wave paths connecting the surface points. The wave travel time is determined from the cross-covariance function of the oscillation signal between different points on the solar surface (Duvall et al., 1993). Because of the stochastic nature of excitation of the oscillations, the cross-covariance function must be averaged over some areas on the solar surface to achieve a signal-to-noise ratio sufficient for measuring the travel times.

A typical cross-covariance function shown in Figure 1b displays several sets of ridges. The lowest set of ridges ('first bounce') corresponds to waves propagated to a particular distance without additional reflections from the solar surface (e.g. AC in Fig. 1a).

Proc. SOHO 10/GONG 2000 Workshop, 'Helio- and Asteroseismology at the Dawn of the Millennium', Santa Cruz de Tenerife, Tenerife, Spain, 2-6 October 2000 (ESA SP-464, January 2001)

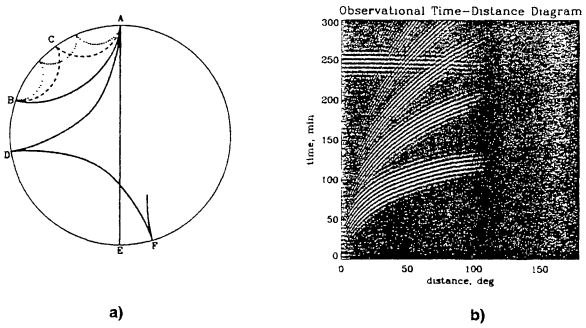

Figure 1. a) A cross-section diagram through the solar interior illustrating the wave propagation inside the Sun. b) The observational cross-covariance function as a function of distance on the solar surface and the delay time. The lowest set of ridges ('first bounce') corresponds to waves propagated to particular distances without additional reflections from the solar surface. The next ridge (second from the bottom) is produced by the waves arriving to the same distances after one reflection from the surface ('second bounce'), and the upper ridges result from the waves arriving after three and more bounces from the surface. The backward ridge associated with the second-bounce ridge is due to the choice of the angular distance range from 0 to 180 degrees.

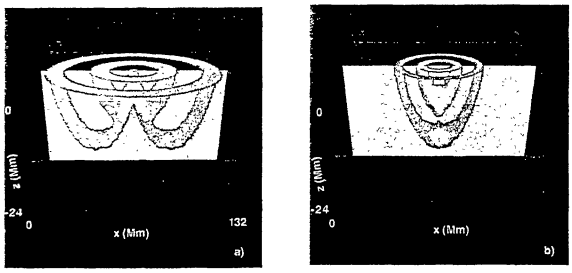

Figure 2. Samples of travel-time sensitivity functions for two schemes of calculations of the cross-covariance function: a) "surface-focusing" scheme in which the central-area oscillation signal is cross-correlated with the signals of surrounding annuli; b) "deep-focusing" scheme in which the signals of the opposite sides of an annulus are cross-correlated. The red color corresponds to high absolute values of the sensitivity functions, and blue color corresponds to the low values. Each picture shows the sensitivity functions for two distances.

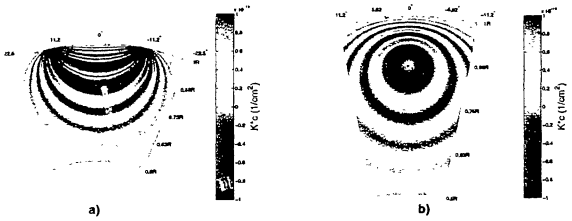

Figure 3. Two cross sections through a 3-D travel-time sensitivity function calculated in the Born approximation: a) along the corresponding ray path which is shown by a solid curve, b) perpendicular to the ray path.

The upper ridges are produced by the waves arriving to the same distance after additional reflections from the surface (e.g. ray path ACB in Fig. 1a corresponds to the 'second bounce' ridge in Fig. 1b). The effects of flows and structural perturbations are separated from each other by taking the difference and the mean of the reciprocal travel times (Kosovichev and Duvall, 1997). Magnetic field causes anisotropy of the mean travel times, which allows us to separate, in principle, the magnetic effects from the variations of the sound speed (or temperature). So far, only a combined effect of the magnetic fields and temperature variations has been measured reliably.

The travel time measured at a point on the solar surface is the result of the cumulative effects of the perturbations in each of the traversed rays of the 3D ray systems. This pattern is then translated for different surface points in the observed area, so that overall the travel times are sensitive to all subsurface points in the depth range 0-20 Mm, in our examples. In a commonly used scheme the travel time is measured between a small central area and a set of surrounding annuli. Examples of the corresponding sensitivity functions are shown in Figure 2a. These measurements are mostly sensitive to a region just beneath the central area. Therefore, the diagnostics of the deep interior in such a "surface-focusing" scheme rely entirely on inversion procedures. Another, scheme initially suggested by Duvall (1995) is based on cross-correlating signals from the opposite sides of the annuli and does not involve the central area. These measurements are mostly sensitive to a small region localized in the deep interior, where the ray paths intersect (Fig. 2b). This "deep-focusing" scheme has many advantages. One of them is that it allows us to study the structure and mass flows directly beneath sunspots without using the oscillation signal inside the spots which may be strongly affected by magnetic fields.

Birch and Kosovichev (2000) have recently developed a wave-theoretical approach for heliotomography based on a Born approximation. Figure 3 shows a travel-time sensitivity kernel in this approximation. Evidently there is significant sensitivity to sound-speed variations outside the ray path. Figure 3b shows the cross section of the kernel perpendicular to the ray path. It turns out that the sensitivity of this kernel along the ray path is exactly zero. A simple spherically symmetrical model (Fig. 4a) for which the travel times can be calculated precisely has been used to test both the ray theory and the Born approximation (Birch and Kosovichev, 2001). It was found that for a large-scale perturbation, with FWHM of 0.2 R (Fig. 4b), both approximations are accurate, but for a small-scale perturbation (0.02

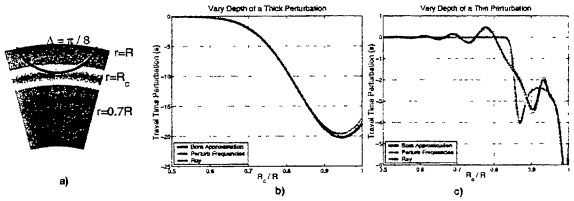

Figure 4. a) Variation of the sound speed in a spherical symmetrical model used for testing the travel-time kernels, R is the solar radius, R_c is the central radius of the perturbation, $\Delta = \pi/8$ is the wave travel distance; b) The travel-time test results for a broad perturbation with FWHM of 0.2 R as a function of the position of the perturbation inside the Sun; c) The same as b) for FWHM of 0.02 R.

R) the ray theory deviates from the exact solution (Fig.4c), resulting in sharper and narrower travel-time variation. This means that when the ray theory is applied to interpretation of real data it underestimates variations of solar parameters and provides oversmoothed images of solar structures. The wave kernels are being incorporated into the inversion procedure. This requires significant computer resources.

3. DIAGNOSTICS OF ACTIVE REGIONS AND COMPLEXES OF ACTIVITY

One of the important tasks of heliotomography is diagnostics of emerging active regions in the interior. For space weather predictions it would be very important to detect active regions before they emerge. However, this task has proven to be very difficult. Here we present the results for an emerging active region observed in January, 1998. This active region (NOAA 8131) was a high-latitude region of the new solar cycle which began in 1997. In Figures 5a-f we show the sound speed variations in a vertical cross-section in the region of the emerging flux and in a horizontal plane at a depth of 18 Mm, for several 8-hour intervals. The perturbations of the magnetosonic speed shown in these figures are associated with the magnetic field and temperature variations in the emerging magnetic structures. It is clear that the 8-hour integration time which yields a good signal-to-noise ratio is not sufficiently short for detecting emerging flux before it appears on the surface. Only reducing the integration time to 2 hours we were able to detect a strong perturbation at the bottom of our observing region (Figure 6). From the investigation of emerging active regions we conclude that it is necessary to probe much deeper layers of the solar convection zone because the emerging flux propagates very rapidly in the top 20 Mm. The estimated emergence speed is approximately 1.3 km/s. This is higher than predicted by theories. The high emergence speed makes the problem of detection of emerging active regions in the solar interior very challenging.

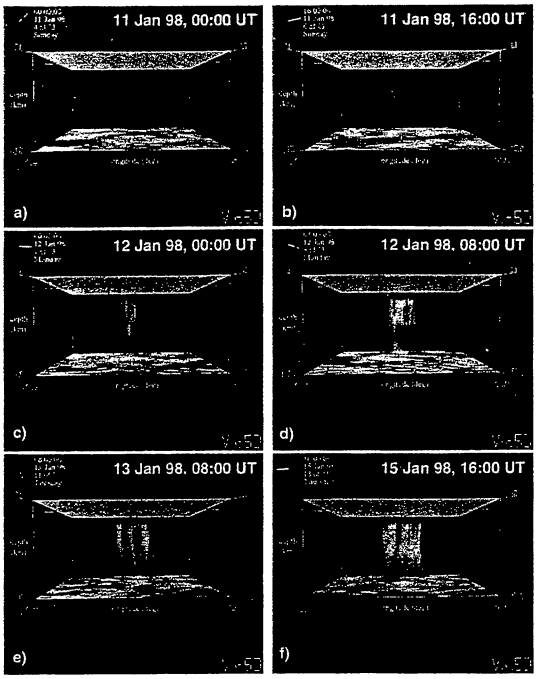

Figure 5. The sound-speed perturbations in the solar convection zone in the emerging active region of January 1998 obtained with 8-hour time resolution. The horizontal size of the box is approximately 38 degrees (460 Mm), the vertical size is 18 Mm. The panels on the top are MDI magnetograms showing the surface magnetic field of positive (red) and negative (blue) polarities. The perturbations of the sound speed are approximately in the range from -1 to +1 km/s. The positive variations are shown in red, and the negative ones in green.

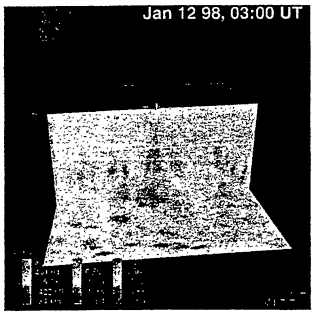

Figure 6. Image of the acoustic wave speed in an emerging active region in the solar convection zone obtained from the SOHO MDI data on January 12, 1998, from 02:00 to 04:00 UT. The horizontal size of the box is approximately 560 Mm, and the depth is 18 Mm. The (mostly) transparent panel on the top is an MDI magnetogram showing the surface magnetic field of positive (red) and negative (blue) polarities stronger than 200 Gauss. The vertical and bottom panels show perturbations of the sound speed (positive in red and negative in blue) which are approximately in the range from -1.3 to +1.3 km/s.

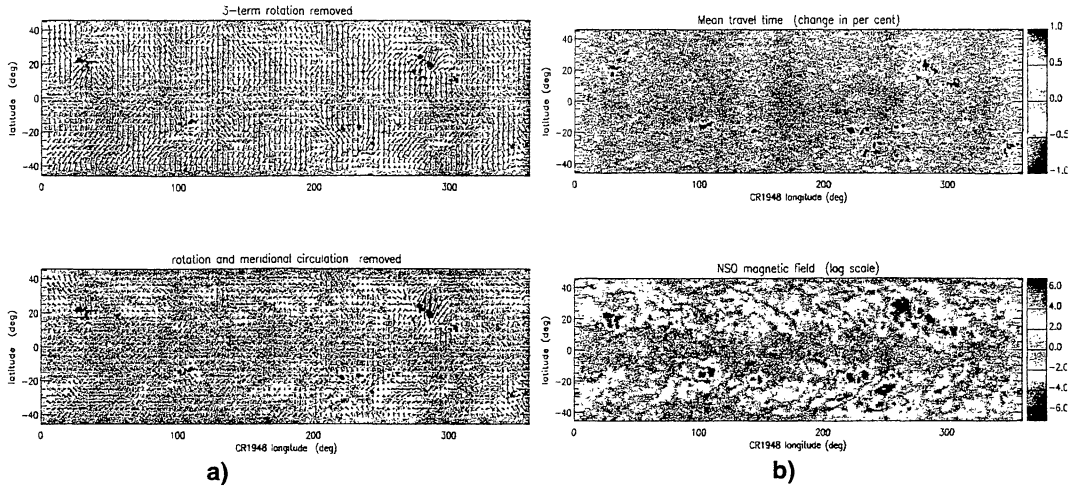

Figure 7. a) Large-scale near-surface flows associated with active regions, obtained from surface gravity waves (f-modes). The background color map shows magnetic field. b) Variations of the f-mode travel times in a near-surface layer. The bottom diagram is the corresponding synoptic magnetic chart (Gizon et al., 2001).

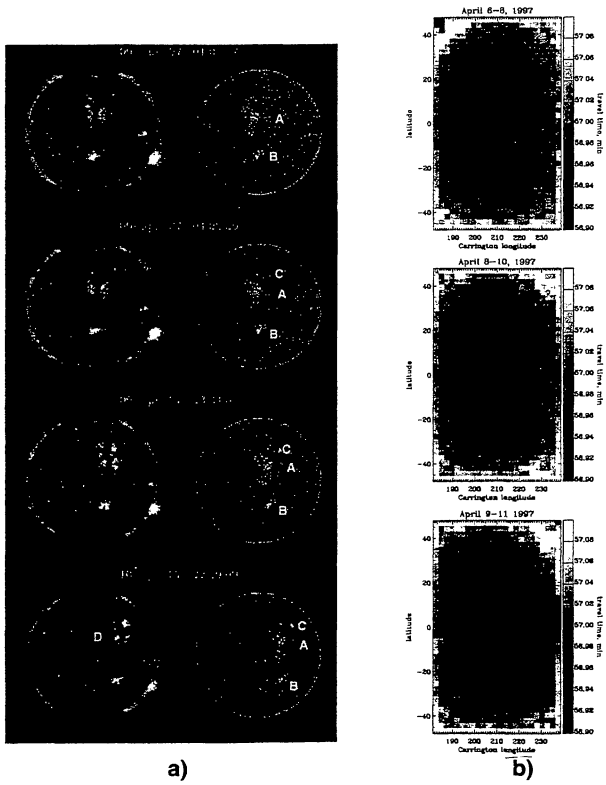

Figure 8. a) The structure of a longitudinal complex of activity observed in April 9-10 1997 by EIT (left column) and MDI (right column). b) Variations of acoustic travel times propagating in the top layer 35 Mm thick for three periods of time in April 6-11, 1997, obtained from MDI medium-l data.

Two other prediction capabilities are being developed. The first one is the detection of new active regions on the far side of the Sun by Lindsey and Braun (2000). Their technique is a version of the "deep-focusing" scheme when the intersection points of acoustic ray paths are chosen on the far side. This approach is very promising for detecting large new active regions before they rotate to the front side of the Sun, and thus for providing new unique data for advanced space weather forecasts. Another capability is based on the detection of surface precursors of new active regions prior their emergence, such as large-scale flow patterns. Kosovichev (1996) and Gizon et al. (2001) have found indications of large-scale converging flows prior the emergence of new active regions. However, the predictive potential of this technique has not been explored.

Duvall and Gizon (2000) have developed a diagnostic of near-surface layers by applying the time-distance approach to surface gravity waves (f modes). These waves are much less sensitive to temperature variations, and therefore the mean travel-differences for these waves are mostly due to magnetic field. The f-mode waves also provide very accurate measurements for horizontal mass flows just beneath the solar surface, in the upper layer 1–2 Mm thick, and allow us to detect both large-scale and small-scale flow patterns associated with solar activity (Gizon et al, 2000). Figure 7a shows large-scale flow patterns during Carrington Rotation 1948 (April 4, 1999 – May 1, 1999). The upper panel shows the flows including zonal flows ("torsional oscillations") and meridional flows; in the bottom panel both zonal and meridional flows are removed. These results reveal converging large-scale flows associated with active regions, with a velocity of $\simeq 50 m/s$. Figure 7b shows the travel-time f-mode signal caused by magnetic fields (top panel) and the corresponding surface magnetic field map (bottom).

Active longitudes play a very important role in the solar cycle. We have attempted to look at the internal structure of a longitudinal complex of activity observed in April 1997 (Fig. 8a). This complex is interesting because it shows emergence of an active region (C) of the new solar cycle at the same longitude which contains a decaying active region (A) of the 'old' cycle (Benevolenskaya et al., 1999).

The diagrams in Fig. 8b show the travel-time variations for three periods of time in April 6-11, 1997. During this period an old active region in the southern hemisphere decayed, and an active region of the new cycle emerged in the northern hemisphere. Prior to the emergence the time-distance measurements reveal a large area of sound-speed perturbation. These measurements cover depths from 0 to 35 Mm. Unfortunately, the full-resolution images are not available for this period, and therefore the travel-time measurements obtained from MDI medium-l data are rather poor. In these data we do not see a connection between the northern and southern parts of the longitudinal complex, which one might expect.

4. DIAGNOSTICS OF SUNSPOTS

After the emergence of new active regions we have observed a gradual increase of the perturbation in the subsurface layers, coincident with the formation of sunspots. In Figure 9 we show an example of the internal structure of a large sunspot of June 20, 1998, inferred by using two different time-distance schemes: "surface-focusing" (Fig. 9a) and "deep-focusing" (Fig. 9b). An image of the spot taken in the continuum is shown at the top. The sound-speed perturbations in the spot are much stronger than in the emerging flux, and reach more than 3 km/s. This corresponds to temperature variations of 2,000-3,000 K or to 10-20 kG magnetic field. These two time-distance schemes provide similar results. The deep-focusing images while being sharper are somewhat noisier than the surface-focusing images.

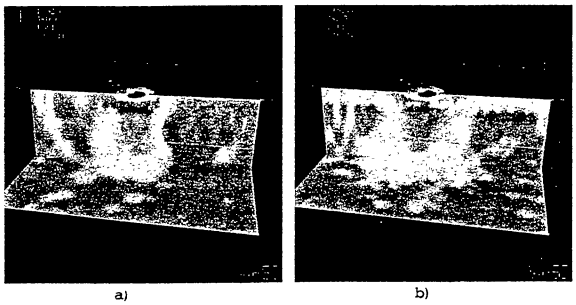

Figure 9. The sound-speed perturbation in a sunspot obtained using the "surface-focusing" (a) and "deep-focusing" (b) schemes. The horizontal size of the box is 13 degrees (158 Mm), the depth is 24 Mm. The positive variations are shown in red, and the negative ones in blue.

Immediately beneath the spot the perturbation to wave speed is negative in the subsurface layers and becomes positive in the deeper interior. One can suggest that the negative perturbations of the wave speed beneath the spot are, probably, due to the lower temperature. These data have revealed 'fingers' - narrow long perturbations which are 4-5 Mm deep and connect pores of the same polarity to the spot (Kosovichev et al, 2000). For both types of measurements the sound-speed signal sharply decreases at a depth of $\sim$ 20 Mm.

We have also found evidence for converging flows beneath the spot, which may play an important role for sunspot stability. Figure 10a shows the sound speed distribution and the flow field in a vertical cut through the sunspot shown in Fig. 9. This result provides evidence of converging flows beneath the spot. Parker (1993) suggested that the field of a sunspot divides into many separate tubes within the first 1000 km below the surface, and that a downdraft beneath the sunspot holds the separate tubes in a loose cluster (Fig. 10b). Recently, a detailed investigation of sunspot flows has been carried out by Zhao et al (2001).

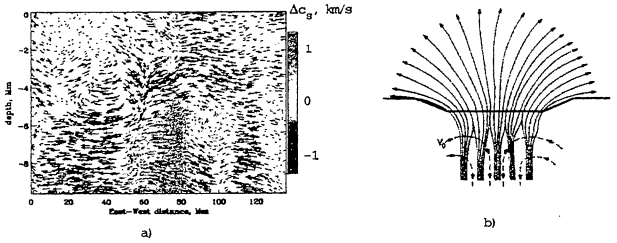

Figure 10. a) Flow pattern around the sunspot in a vertical cut through the upper convection zone. The length of the arrows is proportional to flow velocity. The maximum velocity is approximately 1 km/s. The background color image shows the sound-speed variations in the vertical plane. b) Parker's (1979) model of sunspots.

It is intriguing that the inversion result shows converging flows in the top layer of the sunspot region which are opposite to the well-known diverging Evershed flow observed spectroscopically on the solar surface. Gizon et al. (2000) have studied the horizontal flows in sunspots using the f-mode diagnostics. They found that the f-mode results shown in Figure 11 correspond well to the direct Doppler signal. These results show both the Evershed flow in the penumbra and the moat flow outside the penumbra. Both these flows are directed from the spot. In addition, a reverse flow towards the spot has been found outside the moat flow region. It is likely that a circular downflow region around the sunspot exists where these two flows meet. The velocity amplitude of the Evershed flow inferred from the f-mode is systematically lower than that at the surface. This suggests that the Evershed flow is a shallow phenomenon. This can explain the apparent disagreement with the results obtained from acoustic modes (Fig. 10a).

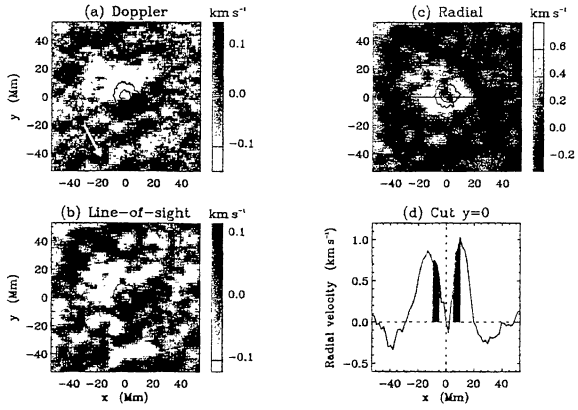

Figure 11. Velocities of near-surface horizontal flows around a sunspot of December 6, 1998, obtained from direct Doppler images (a) and inversion of f-mode travel times (b-d). The maps have a spatial resolution of 1.64 Mm. Panel b) shows the line-of-sight projection of the inferred horizontal velocity field. Panel c) displays the horizontal radial velocity measured from the center of the sunspot; the inferred outflow which surrounds the sunspot (white color) is known as the moat flow. Panel d) shows a cut through panel c) along the horizontal line $y = 0$; the vertical shaded regions indicate the location of the penumbra. Note that two-dimensional wave-theoretical sensitivity kernels (first Born approximation) were used in the inversion of f-mode travel times (Gizon et al., 2000).

Using MDI continuum intensity images we have also looked at possible variations of irradiance associated with the sunspot structure. Of particular interest are bright rings around sunspots also observed by Rast et al (1999). The MDI images reveal bright rings at the outer boundary of the moat flow (Fig. 12). Relations between local irradiance variations and sunspot dynamics have not been established.

5. CONCLUSIONS

Heliotomography provides a unique tool for studying the birth and evolution of active regions and sunspots. It also provides important information for space weather forecasts by detecting sound-speed variations in the interior associated with emerging active regions, by observing new active regions on the far side of the sun, and by determining characteristics of large-scale flows which give indirect evidence for new active regions. The tomographic imaging of a large sunspot supports the idea that sunspots consist of strong magnetic field flux tubes which are held together by converging flows. A theory of solar acoustic and surface waves based on a Born approximation provides a robust basis for developing quantitative 3-D diagnostics of the solar interior.

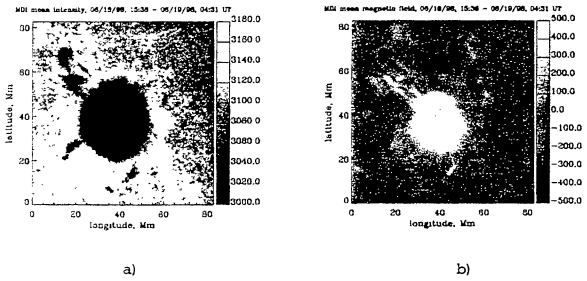

Figure 12. a) MDI continuum intensity image of a sunspot averaged for 13 hours; b) MDI magnetogram of the same sunspot for the same period of time.

REFERENCES

Benevolenskaya, E.E., Kosovichev, A.G. & Scherrer, P.H., 1999, *Sol. Phys.*, **190**, 145.

Birch, A.C. & Kosovichev, A.G., 2000, *Sol. Phys.*, **192**, 193.

Birch, A.C. & Kosovichev, A.G., 2001, in Proc. IAU Symp. 203, *Recent Insights into the Physics of the Sun and Heliosphere - Highlights from SOHO and Other Space Missions*, ed. P. Brekke, B. Fleck & J. B. Gurman (San Francisco: ASP).

Duvall T.L., Jr., Jefferies, S. M., Harvey, J. W., & Pomerantz, M. A., 1993, *Nature*, **362**, 430.

Duvall T.L., Jr., 1995 *GONG '94: Helio- and Astero-Seismology from the Earth and Space*, Roger K. Ulrich, Edward J. Rhodes, Jr., Werner Däppen (eds), **76**, 465.

Duvall T.L. & Gizon L., 2000, *Sol. Phys.*, **192**, 177.

Gizon L., Duvall T.L. & Larsen R.M., 2000, *Journal of Astrophysics and Astronomy*, in press.

Gizon L., Duvall T.L. & Larsen R.M., 2001, in Proc. IAU Symp. 203, *Recent Insights into the Physics of the Sun and Heliosphere - Highlights from SOHO and Other Space Missions*, ed. P. Brekke, B. Fleck & J. B. Gurman (San Francisco: ASP).

Kosovichev, A.G., 1996, *ApJ*, **461**, L55.

Kosovichev, A.G. & Duvall, T.L., Jr., 1997, *SCORe'96 : Solar Convection and Oscillations and their Relationship*, Eds.: F.P. Pijpers, J. Christensen-Dalsgaard, & C.S. Rosenthal, Kluwer Academic Publishers (Astrophysics and Space Science Library Vol. 225), p. 241.

Kosovichev, A. G., Duvall, T. L. & Scherrer, P. H., 1999, *Adv. Space Res.*, **24**, p. 163.

Kosovichev, A. G., Duvall, T. L. & Scherrer, P. H., 2000, *Sol. Phys.*, **192**, 159.

Lindsey, C. & Braun, D.C., 2000, *Science*, **287**, 1799.

Parker, E. N., 1993, *ApJ*, **230**, 905.

Rast, M. et al, 2000, Nature, **401**, 678.

Zhao, Junwei, Kosovichev, A.G. & Duvall, T.L., Jr, 2001, *ApJ*, submitted.